IP_3R2-independent Ca^{2+} release from the endoplasmic reticulum in astrocytes

Yohei Okubo[1]*, Kazunori Kanemaru[1, 2], Junji Suzuki[3], Kenta Kobayashi[4, 5], Kenzo Hirose[6] & Masamitsu Iino[2]*

[1]Department of Pharmacology, Graduate School of Medicine, The University of Tokyo, Tokyo 133-0033, Japan
[2]Department of Cellular and Molecular Pharmacology, Nihon University School of Medicine, Tokyo 173-8610, Japan.
[3]Department of Physiology, University of California at San Francisco, San Francisco, CA 94143, USA
[4]Section of Viral Vector Development, National Institute for Physiological Sciences, Okazaki 444-8585, Japan.
[5]The Graduate University for Advanced Studies (SOKENDAI), Hayama 240-0193, Japan.
[6]Department of Neurobiology, Graduate School of Medicine, The University of Tokyo, Tokyo 133-0033, Japan

*Corresponding authors: Yohei Okubo & Masamitsu Iino
YO: Department of Pharmacology, Graduate School of Medicine, The University of Tokyo, 7-3-1 Hongo, Bunkyo-ku, Tokyo 113-0033, Japan.
E-mail: yoheio@m.u-tokyo.ac.jp, Tel: +81-3-5841-3414, Fax: +81-3-5841-3390
MI: Department of Cellular and Molecular Pharmacology, Nihon University School of Medicine, 30-1, Oyaguchi Kami-cho, Itabashi-ku, Tokyo 173-8610, Japan.
E-mail: iino@m.u-tokyo.ac.jp, Tel: +81-3-3972-8111

The authors declare no competing financial interests.

Abstract

Accumulating evidence indicates that astrocytes are actively involved in the physiological and pathophysiological functions of the brain. Intracellular Ca^{2+} signaling, especially Ca^{2+} release from the endoplasmic reticulum (ER), is considered to be crucial for the regulation of astrocytic functions. Mice with genetic deletion of IP_3R type 2 (IP_3R2) are reportedly devoid of astrocytic Ca^{2+} signaling, and thus widely used to explore the roles of Ca^{2+} signaling in astrocytic functions. While functional deficits in IP_3R2-knockout (KO) mice have been found in some reports, no functional deficit was observed in others. Thus, there remains a controversy regarding the functional significance of astrocytic Ca^{2+} signaling. To address this controversy, we re-evaluated the assumption that Ca^{2+} release from the ER is abolished in IP_3R2-KO astrocytes using a highly sensitive imaging technique. We expressed the ER luminal Ca^{2+} indicator G-CEPIA1*er* in cortical and hippocampal astrocytes to directly visualize spontaneous and stimulus-induced Ca^{2+} release from the ER. We found attenuated but significant Ca^{2+} release in response to application of norepinephrine to IP_3R2-KO astrocytes. This IP_3R2-independent Ca^{2+} release induced only minimal cytosolic Ca^{2+} transients but induced significant Ca^{2+} increases in mitochondria that are frequently in close contact with the ER. These results indicate that ER Ca^{2+} release is retained and is sufficient to increase the Ca^{2+} concentration in close proximity to the ER in IP_3R2-KO astrocytes.

Introduction

Accumulating evidence indicates that astrocytes play not only trophic and supportive roles but also active roles in the physiological and pathophysiological functions of the brain (Volterra and Meldolesi, 2005; Barres, 2008). Therefore, clarifying the mechanisms for regulation of astrocytic functions has become a crucial issue in neuroscience. Intracellular Ca^{2+} signaling has attracted attention because astrocytes show robust spontaneous and stimulus-induced Ca^{2+} transients (Verkhratsky et al., 1998; Bazargani and Attwell, 2016).

Ca^{2+} release from the endoplasmic reticulum (ER) via inositol 1,4,5-trisphosphate receptor (IP_3R) has been recognized as a major component of spontaneous and G_q-coupled receptor-induced Ca^{2+} signaling in astrocytes. Therefore, to explore the significance of astrocytic Ca^{2+} signaling, mice with genetic deletion of IP_3R type 2 (IP_3R2) (Li et al., 2005), which is enriched in astrocytes (Sharp et al., 1999; Holtzclaw et al., 2002; Zhang et al., 2014), have been widely used. In IP_3R2-knockout (KO) mice, Ca^{2+} transients in astrocytes were considered to be absent based on an imaging study of cytosolic Ca^{2+} transients by fluorescent Ca^{2+} indicator dyes (Petravicz et al., 2008). Physiological and pathophysiological phenotypes have been observed in IP_3R2-KO mice, including plasticity and learning (Takata et al., 2011; Chen et al., 2012; Navarrete et al., 2012; Perez-Alvarez et al., 2014; Padmashri et al., 2015; Kim et al., 2016; Monai et al., 2016; Yang et al., 2016), homeostasis of K^+ (Wang et al., 2012a, 2012b), pathogenesis of stroke, traumatic brain injury and neurodegenerative disease (Dong et al., 2013; Kanemaru et al., 2013; Li et al., 2015; Rakers and Petzold, 2016; Saito et al., 2018), and depression-like behaviors (Cao et al., 2013). However, several studies have reported no changes in basal synaptic activity and behavior (Petravicz et al., 2008, 2014; Agulhon et al., 2013), hippocampal synaptic plasticity (Agulhon et al., 2010), and neurovascular coupling (Nizar et al., 2013; Takata et al., 2013; Bonder and McCarthy, 2014) in IP_3R2-KO mice. These contradictory results have caused confusion about the functional

significance of Ca^{2+} signaling in astrocytes (Hamilton and Attwell, 2010; Fiacco and McCarthy, 2018; Savtchouk and Volterra, 2018).

One of the possible explanations that can resolve this controversy is that IP_3R2-independent Ca^{2+} signaling exists and contributes to the functions of IP_3R2-KO astrocytes. In fact, recent studies using genetically encoded Ca^{2+} indicators (GECIs) have clearly shown the presence of Ca^{2+} signals in IP_3R2-KO astrocytes (Kanemaru et al., 2014; Srinivasan et al., 2015; Rungta et al., 2016; Agarwal et al., 2017). These IP_3R2-independent Ca^{2+} transients were thought to be mediated by Ca^{2+} influx via the plasma membrane (Shigetomi et al., 2012; Srinivasan et al., 2015; Rungta et al., 2016) or Ca^{2+} release from mitochondria (Agarwal et al., 2017). These studies suggest that increases in the concentration of Ca^{2+} originating from sources other than the ER may regulate the functions of astrocytes. However, it remains elusive whether ER Ca^{2+} release is completely abolished in IP_3R2-KO astrocytes.

We thus examined whether IP_3R2-independent Ca^{2+} release from the ER is present in IP_3R2-KO astrocytes. Because cytosolic Ca^{2+} transients can be generated by Ca^{2+} derived from sources other than the ER, we directly detected ER Ca^{2+} release as a decrease in the Ca^{2+} concentration within the ER ($[Ca^{2+}]_{ER}$). We recently developed a series of calcium-measuring organelle-entrapped protein indicators (CEPIAs) that allow visualization of Ca^{2+} dynamics within the ER and mitochondria with a high signal-to-noise ratio (Suzuki et al., 2014, 2016; Okubo et al., 2015). In this study, we expressed the ER Ca^{2+} indicator G-CEPIA1*er* in cortical and hippocampal astrocytes of IP_3R2-KO mice. We found attenuated but significant Ca^{2+} release from the ER. We also used the mitochondrial Ca^{2+} indicator CEPIA2*mt* and successfully observed significant Ca^{2+} transfer into mitochondria from the ER in IP_3R2-KO astrocytes. These findings allowed us to reinterpret the results from IP_3R2-KO mice and shed new light on the significance of astrocytic Ca^{2+} signaling.

Materials and Methods

Animals

All animal experiments were carried out in accordance with the regulations and guidelines of the Institutional Animal Care and Use Committee at The University of Tokyo and were approved by the Institutional Review Committee of the Graduate School of Medicine, The University of Tokyo. C57BL/6 mice were used as wild-type (WT) mice. IP_3R2-KO mice (Li et al., 2005) were obtained from J. Chen (University of California at San Diego). Mice were kept under a 12 h light/dark cycle with *ad libitum* access to food and drinking water.

Preparation of viral vectors

To generate adeno-associated viruses (AAVs) for astrocyte-specific expression of GECIs, the cytomegalovirus promoter of pAAV-MCS (AAV Helper Free Expression System, Cell Biolabs, Inc., San Diego, CA) was replaced with the gfaABC_1D astrocyte-specific promoter derived from pZac2.1-gfaABC1D-Lck-GCaMP3 (Shigetomi et al., 2013). G-CEPIA1*er*, CEPIA2*mt*, GCaMP6f, and ER-YFP were inserted downstream of the gfaABC_1D promoter to generate pAAV-gfaABC_1D-G-CEPIA1*er*, pAAV-gfaABC_1D-CEPIA2*mt*, pAAV-gfaABC_1D-GCaMP6f, and pAAV-gfaABC_1D-ER-YFP. AAV5 vectors were packaged using the AAV Helper Free Expression System. The packaging plasmids (pAAV-RC5 and pHelper) and transfer plasmid (pAAV-gfaABC_1D-G-CEPIA1*er*, pAAV-gfaABC_1D-CEPIA2*mt*, pAAV-gfaABC_1D-GCaMP6f, or pAAV-gfaABC_1D-ER-YFP) were transfected into HEK293T cells using the calcium phosphate method. The medium was replaced at 18 h after transfection with fresh medium, and the cells were incubated for 48 h. Harvested cells were lysed by repeated freezing and thawing, and a crude cell extract containing AAV5 vector particles was obtained. AAV5 vector particles were purified by ultracentrifugation with cesium chloride. The purified particles were dialyzed against PBS

and then concentrated by ultrafiltration using an Amicon 10K MWCO filter (Merck Millipore, Darmstadt, Germany). The copy number of the viral genome (vg) was determined by real-time quantitative PCR.

AAV injection

Male C57BL/6 mice or IP_3R2-KO mice (postnatal day 56–120) were anesthetized with isoflurane (induction at 5%, maintenance at 1–2%, vol/vol, MK-A100, Muromachi, Kyoto, Japan). The mice were placed in a stereotaxic frame (SR-5M-HT, Narishige, Tokyo, Japan). The skull was thinned (about 1 mm in diameter) above the right parietal cortex using a burr powered by a high speed drill (ULTIMATE XL-D, NSK, Kanuma, Japan). AAV5-gfaABC$_1$D-G-CEPIA1*er* (0.98 or 1.3 × 10^{13} vg ml^{-1}), AAV5-gfaABC$_1$D-CEPIA2*mt* (0.98 × 10^{13} vg ml^{-1}), AAV5-gfaABC$_1$D-GCaMP6f (1.1 × 10^{13} vg ml^{-1}), or pAAV-gfaABC$_1$D-ER-YFP (3.0 × 10^{13} vg ml^{-1}) was unilaterally injected into the cortex (1.5–2 mm posterior to the bregma, 1–1.5 mm lateral to the midline, and 300 μm from the surface) or hippocampus (2 mm posterior to the bregma, 1.5 mm lateral to the midline, and 1.6 mm from the surface) through glass pipettes. A viral solution (1 μL) was delivered at a rate of 200 nL min^{-1} using a micropump (Legato 130, KD scientific, Holliston, MA). Glass pipettes were left in place for at least 10 min. Mice were sacrificed at 14–28 days after AAV injection for imaging and immunohistochemistry.

Preparation of brain slices and imaging

Coronal cortical or hippocampal slices (300 μm in thickness) were prepared as described previously (Edwards et al., 1989). Slices were prepared in ice-cold artificial cerebrospinal fluid (ACSF) bubbled with 95% O_2 and 5% CO_2 using a vibrating slicer (PRO7, Dosaka, Kyoto, Japan). Slices were incubated in a holding chamber containing ACSF bubbled with

95% O_2 and 5% CO_2 at 35°C for 1 h and then returned to 23°C. ACSF contained (in mM) 125 NaCl, 2.5 KCl, 2 $CaCl_2$, 1 $MgSO_4$, 1.25 NaH_2PO_4, 26 $NaHCO_3$, and 20 glucose. Imaging was carried out with a two-photon microscope (TSC MP5, Leica, Wetzlar, Germany) equipped with a water immersion objective (×25, NA 0.95, HCS IR APO, Leica) and Ti:sapphire laser (MaiTai DeepSee; Spectra Physics, Santa Clara, CA). Slices were transferred to a recording chamber under a microscope and continuously perfused with ACSF bubbled with 95% O_2 and 5% CO_2. Tetrodotoxin (1 μM) was added to ACSF to inhibit neuronal activities throughout imaging. Norepinephrine (NE, 10 μM) and cyclopiazonic acid (CPA, 50 μM) were dissolved in ACSF and administered through the perfusion system of the recording chamber. The excitation wavelength was 900–920 nm. Emitted fluorescence was filtered by a 500–550 nm barrier filter and detected with photomultiplier tubes. Data were acquired in time lapse XY-scan mode (0.2–0.5 Hz). Experiments were carried out at room temperature (22–24°C).

Immunohistochemistry

After anesthetization with pentobarbital, mice were fixed by perfusion of PBS containing 4% paraformaldehyde (PFA). The isolated brain was postfixed with 4% PFA for 1 h at 4°C and cryoprotected with 20% sucrose overnight. Brain sections (20 μm) prepared with a cryomicrotome (CM1200; Leica) were permeabilized and blocked with PBS containing 0.2% Triton X-100, 10% FBS, and 1% BSA for 1 h at room temperature. After incubation with antibodies for green fluorescent protein (monoclonal; GF090R, 1:100; NACALAI TESQUE) and glial fibrillary acidic protein (GFAP, polyclonal; G9269, 1:20; Sigma) overnight at 4°C, the sections were stained with Alexa Fluor 546- or 647-labeled goat anti-mouse or anti-rabbit IgG antibody (1:200; Invitrogen) for 1 h at room temperature. Sections were imaged using a confocal microscope (LEICA TCS SP8; Leica) equipped with an oil-immersion objective (63×, NA = 1.4).

Data analysis

Data were analyzed using ImageJ software. Astrocytes were analyzed in layer 2/3 of the cortex or in the CA1 stratum radiatum of the hippocampus. Fluorescence intensities were corrected for background fluorescence by measuring a non-fluorescent area and normalized by the average of the first 10 or 20 frames to calculate the fractional changes in fluorescence intensity ($\Delta F/F_0$). Spontaneous G-CEPIA1*er* responses were manually detected and analyzed. Fluorescence changes with a rate of decrease faster than -0.015 $\Delta F/F_0$ s^{-1} and amplitude larger than -0.05 $\Delta F/F_0$ were defined as responses. Synchronous decreases in G-CEPIA1*er* fluorescence throughout a single astrocyte were defined as global responses. Localized fluorescence decreases with about 10–15 μm in diameter at the process region were defined as process-localized responses. The amplitude of spontaneous G-CEPIA1*er* responses was measured after smoothing time courses of $\Delta F/F_0$ by a moving average with five frame windows. The amplitude of NE-induced G-CEPIA1*er*, CEPIA2*mt*, GCaMP6f, or ER-YFP responses was defined as the average of $\Delta F/F_0$ within the 3-min time window starting from the start of NE application. The amplitude of the CPA-induced G-CEPIA1*er* fluorescence decrease was defined as the $\Delta F/F_0$ value in a steady state.

Results

G-CEPIA1*er* detects Ca^{2+} release from the ER in cortical astrocytes of IP_3R2-KO mice

We used a serotype 5 AAV carrying the minimal astrocyte-specific gfaABC$_1$D promoter to express G-CEPIA1*er* in astrocytes of the adult mouse cortex. Immunohistochemical analysis indicated co-localization of G-CEPIA1*er* and the astrocyte marker GFAP (Fig. 1A), confirming the astrocyte specificity of AAV5-gfaABC$_1$D-mediated expression (Shigetomi et al., 2013). At subcellular levels, expression of G-CEPIA1*er* was observed throughout the soma and processes, although localization at the tips of ramified processes was unclear (Fig. 1A). This G-CEPIA1*er* distribution was consistent with a report on the distribution pattern of the ER in astrocytes (Patrushev et al., 2013).

To analyze Ca^{2+} release from the ER, G-CEPIA1*er*-expressing layer 2/3 astrocytes in acute cortical slice preparations were imaged using a two-photon microscope. Application of CPA, a sarco/endoplasmic reticulum Ca^{2+}-ATPase (SERCA) inhibitor, was used to deplete Ca^{2+} within the ER. CPA-induced Ca^{2+} depletion resulted in a marked decrease in the G-CEPIA1*er* fluorescence intensity of both WT and IP_3R2-KO astrocytes, confirming that G-CEPIA1*er* reports ER Ca^{2+} levels (Fig. 1B). There was no significant difference in the amplitudes of the CPA-induced G-CEPIA1*er* fluorescence decrease between WT and IP_3R2-KO astrocytes, indicating that the basal $[Ca^{2+}]_{ER}$ in IP_3R2-KO astrocytes was similar to that in WT astrocytes (Fig. 1B). However, the rate of decrease in $[Ca^{2+}]_{ER}$ was greater in WT astrocytes than in IP_3R2-KO astrocytes (Fig. 1B). In WT astrocytes, $[Ca^{2+}]_{ER}$ was often decreased in a stepwise manner as shown in Fig. 1B. Each step appeared to reflect spontaneous Ca^{2+} release events via IP_3R2 as described in the following.

We next investigated G_q-coupled receptor-induced Ca^{2+} release from the ER in astrocytes. NE, which is released from the axons of locus coeruleus neurons, induces significant ER Ca^{2+} release through activation of α_1-adrenergic receptors in astrocytes *in vivo*

(Ding et al., 2013; Paukert et al., 2014; Srinivasan et al., 2015). Although previous studies have shown that NE-induced Ca^{2+} release is absent in IP_3R2-KO astrocytes, we re-evaluated this result using G-CEPIA1*er*. Bath application of NE (10 μM) induced a large decrease in $[Ca^{2+}]_{ER}$ of WT astrocytes, indicating robust Ca^{2+} release from the ER (Fig. 2A and B). Following washout of NE, there was slow recovery of $[Ca^{2+}]_{ER}$ due to Ca^{2+} reuptake by the ER. The time course was consistent with ER Ca^{2+} dynamics induced by IP_3R-mediated Ca^{2+} release in other cell types shown in our previous studies (Suzuki et al., 2014; Okubo et al., 2015). NE-induced $[Ca^{2+}]_{ER}$ responses showed almost the same amplitude and time course in the soma and processes, indicating induction of cell-wide Ca^{2+} releases in response to bath application of NE (Fig. 2A, B and D). To our surprise, NE application induced a smaller but significant decrease in $[Ca^{2+}]_{ER}$ of IP_3R2-KO astrocytes throughout the soma and processes (Fig. 2A, B and D). This observation clearly indicates that ER Ca^{2+} release is not completely abolished in IP_3R2-KO astrocytes.

Most GECIs including G-CEPIA1*er* are sensitive to pH. To exclude the possibility that the observed changes in the G-CEPIA1*er* fluorescence intensity was due to a change in pH within the ER, we expressed ER-localized YFP that is sensitive to pH but insensitive to Ca^{2+} (Suzuki et al., 2014). ER-YFP showed no response to NE in either WT or IP_3R2-KO astrocytes, confirming that NE-induced G-CEPIA1*er* responses reflected decreases in $[Ca^{2+}]_{ER}$ (Fig. 2C and D).

G-CEPIA1*er* detects spontaneous Ca^{2+} release in WT astrocytes

During our observation of $[Ca^{2+}]_{ER}$ in WT astrocytes, we found spontaneous decreases in $[Ca^{2+}]_{ER}$ (Fig. 3). There were two types of spontaneous events: a “global” response that showed a synchronous decrease in $[Ca^{2+}]_{ER}$ throughout the astrocyte (Fig. 3A and D), and a “process-localized” response that was localized at processes with diameters of about 10–15

μm (Fig. 3B and D). These Ca^{2+} release dynamics may at least partly correspond to cell-wide and localized Ca^{2+} signals imaged by cytosolic Ca^{2+} indicators in previous studies (Kanemaru et al., 2014; Srinivasan et al., 2015), although precise correlations require further analyses. However, we did not find spontaneous $[Ca^{2+}]_{ER}$ responses in IP_3R2-KO astrocytes (Fig. 3C). Thus, in IP_3R2-KO astrocytes, spontaneous Ca^{2+} release events, if any, appeared to be attenuated to a level undetectable by G-CEPIA1*er*.

Cytosolic Ca^{2+} transients are mediated by IP_3R2-independent Ca^{2+} release

To clarify the significance of IP_3R2-independent Ca^{2+} release in the intracellular Ca^{2+} signaling of astrocytes, we investigated changes in the cytosolic Ca^{2+} concentration ($[Ca^{2+}]_{Cyt}$) in response to NE application (Fig. 4). Cytosolic Ca^{2+} indicator GCaMP6f (Chen et al., 2013) was expressed in astrocytes using an AAV, showing a diffuse distribution throughout the cytosol (Fig. 4A). Application of NE induced large and cell-wide $[Ca^{2+}]_{Cyt}$ responses in WT astrocytes (Fig. 4B and C). These NE-induced $[Ca^{2+}]_{Cyt}$ responses showed no significant subcellular distribution, but were synchronized throughout the cell. Responses were abolished after treatment with CPA, indicating a critical contribution of ER Ca^{2+} release to NE-induced $[Ca^{2+}]_{Cyt}$ transients (Fig. 4B and C). We also observed spontaneous and spatially confined $[Ca^{2+}]_{Cyt}$ responses that probably correspond to previously reported "Ca^{2+} twinkle" or "microdomain" Ca^{2+} signals (Kanemaru et al., 2014; Srinivasan et al., 2015). These localized $[Ca^{2+}]_{Cyt}$ signals hardly contributed to $\Delta F/F_0$ traces of GCaMP6f averaged within the entire cell.

In IP_3R2-KO astrocytes, NE induced very small $[Ca^{2+}]_{Cyt}$ responses (Fig. 4B and C). Only very few IP_3R2-KO astrocytes showed clear but relatively small responses. These $[Ca^{2+}]_{Cyt}$ responses in IP_3R2-KO astrocytes were also abolished after treatment with CPA (Fig.

4B and C). These results indicate that IP_3R2-independent Ca^{2+} release, which was detected by G-CEPIA1*er*, did not always increase $[Ca^{2+}]_{Cyt}$ to a level detectable by GCaMP6f.

Significant Ca^{2+} transients in mitochondria are mediated by IP_3R2-independent Ca^{2+} release

We next examined whether IP_3R2-independent Ca^{2+} release contributed to astrocytic Ca^{2+} signaling other than cell-wide cytosolic Ca^{2+} transients. To this end, we focused on mitochondria. The ER and mitochondria often form close contacts where Ca^{2+} is efficiently transferred from the ER to mitochondria without a global increase in $[Ca^{2+}]_{Cyt}$ (Rizzuto et al., 1998; de Brito and Scorrano, 2010; Hirabayashi et al., 2017). We thus investigated changes in the Ca^{2+} concentration within mitochondria ($[Ca^{2+}]_{Mito}$) using CEPIA2*mt*, a Ca^{2+} indicator for the mitochondrial matrix (Suzuki et al., 2014) (Fig. 5). AAV-mediated expression of CEPIA2*mt* in astrocytes resulted in a punctate distribution of fluorescence, which was consistent with the morphology of mitochondria (Fig. 5A). Application of NE to release Ca^{2+} from the ER induced an increase in $[Ca^{2+}]_{Mito}$ of WT astrocytes (Fig. 5B and C). A fraction of WT astrocytes did not show a response as observed in HeLa cells in our previous study (Suzuki et al., 2014) (Fig. 5B and C). The NA-induced $[Ca^{2+}]_{Mito}$ response was abolished after treatment with CPA to deplete the ER (Fig. 5B and C). These results indicate that Ca^{2+} enters mitochondria following Ca^{2+} release from the ER in WT astrocytes. We did not observe subcellular heterogeneity in the NE-induced $[Ca^{2+}]_{Mito}$ responses.

Of note, NE also induced $[Ca^{2+}]_{Mito}$ responses in IP_3R2-KO astrocytes (Fig. 5B and C). Similar to WT astrocytes, a fraction of IP_3R2-KO astrocytes showed no responses. Compared with the minimal $[Ca^{2+}]_{Cyt}$ responses, $[Ca^{2+}]_{Mito}$ showed attenuated but significant responses in IP_3R2-KO astrocytes in response to NE. These $[Ca^{2+}]_{Mito}$ responses in IP_3R2-KO astrocytes were also abolished after treatment with CPA (Fig. 5B and C). These results indicate that

IP_3R2-independent Ca^{2+} release efficiently induces an increase in $[Ca^{2+}]_{Mito}$, and suggest that IP_3R2-independent Ca^{2+} release increases the local Ca^{2+} concentration in the vicinity of the ER.

IP_3R2-independent Ca^{2+} release in hippocampal astrocytes

Regional differences in the properties of astrocytes have been reported (Chai et al., 2017). To investigate whether IP_3R2-independent Ca^{2+} release could be observed in astrocytes of brain regions other than the cortex, we visualized Ca^{2+} release from the ER in hippocampal astrocytes (Fig. 6). G-CEPIA1*er* was expressed in hippocampal astrocytes using an AAV. G-CEPIA1*er*-expressing astrocytes in the CA1 stratum radiatum of acute hippocampal slice preparations were imaged by two-photon microscopy. “Global” and “process localized” spontaneous G-CEPIA1*er* responses were observed in WT astrocytes, but not in IP_3R2-KO astrocytes, which was consistent with the results in cortical astrocytes (Fig. 6A–D). Application of NE induced large G-CEPIA1*er* responses in WT astrocytes, whereas attenuated but significant G-CEPIA1*er* responses were observed in IP_3R2-KO astrocytes (Fig. 6E). Therefore, IP_3R2-independent Ca^{2+} release was commonly observed in cortical and hippocampal astrocytes of IP_3R2-KO mice.

Discussion

In this study, we showed Ca^{2+} release from the ER in IP_3R2-KO astrocytes for the first time. This IP_3R2-independent Ca^{2+} release was effective to increase the Ca^{2+} concentration within mitochondria that make close contacts with the ER. These results provide new insights into the functional significance of ER Ca^{2+} release in astrocytes. The controversy derived from the assumption that ER Ca^{2+} release is abolished in IP_3R2-KO astrocytes should be re-evaluated considering the presence of IP_3R2-independent Ca^{2+} release.

Highly sensitive and specific detection of ER Ca^{2+} release using G-CEPIA1*er*

Although IP_3R2-independent Ca^{2+} release from the ER in IP_3R2-KO astrocytes was detectable by G-CEPIA1*er* responses, the resulting changes in $[Ca^{2+}]_{Cyt}$ were only barely detected by GCaMP6f responses. The difficulty in detecting the $[Ca^{2+}]_{Cyt}$ response is consistent with previous reports that failed to detect evoked $[Ca^{2+}]_{Cyt}$ responses in IP_3R2-KO astrocytes (Petravicz et al., 2008, 2014, Agulhon et al., 2010, 2013; Nizar et al., 2013; Takata et al., 2013). These results suggest that the amount of Ca^{2+} release sufficient to change free $[Ca^{2+}]_{ER}$ is often insufficient to change free $[Ca^{2+}]_{Cyt}$. There appear to be some potential reasons. First, the volume occupied by the smooth ER is about 10% of the cytoplasm (Paumgartner et al., 1981). Therefore, Ca^{2+} released from the ER is diluted in the cytosol. Another possible reason is the Ca^{2+} buffering capacity k (a change in the total Ca^{2+} concentration in a subcellular compartment divided by the corresponding change in free Ca^{2+} concentration in the compartment). In many cell types, cytosolic k is estimated to be 10–1000 (Neher, 1995; Mogami et al., 1999). In pancreatic acinar cells, k of the ER is estimated to be two orders of magnitude smaller than that of cytosol (Mogami et al., 1999). If k is similarly lower in the ER than in the cytosol, this would also reduce the change in $[Ca^{2+}]_{Cyt}$. Therefore, G-CEPIA1*er* is expected to report ER Ca^{2+} release with higher sensitivity than cytosolic Ca^{2+} indicators.

Furthermore, G-CEPIA1*er* can specifically detect ER Ca^{2+} release, whereas cytosolic Ca^{2+} indicators do not specify the source of Ca^{2+}.

Ca^{2+} channels that mediate IP_3R2-independent Ca^{2+} release

Although IP_3R2 is the major ER Ca^{2+} release channel in astrocytes, expression of IP_3R1 and/or IP_3R3 in astrocytes has been indicated by transcriptome analyses (Cahoy et al., 2008; Zhang et al., 2014; Chai et al., 2017) and immunohistochemical studies (Yamamoto-Hino et al., 1995; Sharp et al., 1999). Furthermore, comparison between IP_3R2-KO mice and IP_3R2/IP_3R3-double KO mice indicate a functional contribution of IP_3R3 to astrocytic Ca^{2+} signaling, albeit small (Tamamushi et al., 2012; Sherwood et al., 2017). These previous studies suggest the presence of IP_3-induced Ca^{2+} release via IP_3R1 and/or IP_3R3 in IP_3R2-KO astrocytes.

In addition, expression of ryanodine receptor type3 (RyR3) in astrocytes has been reported (Matyash et al., 2002; Chai et al., 2017). Furthermore, the functional significance of RyR3 was reported in both astrocytic Ca^{2+} signaling and motility (Matyash et al., 2002). Therefore, it also appears possible that Ca^{2+}-induced Ca^{2+} release via RyR3 enhances Ca^{2+} release from the ER in collaboration with IP_3R1 and/or IP_3R3-dependent Ca^{2+} release in astrocytes.

Contribution of IP_3R2-independent Ca^{2+} release to Ca^{2+} signaling in IP_3R2-KO astrocytes

When the extent of the NE-induced increase in Ca^{2+} concentration was compared between WT and IP_3R2-KO astrocytes, there was a much higher Ca^{2+} increase in mitochondria than in the cytoplasm of IP_3R2-KO astrocytes (Figs. 4 and 5). These results suggest a mechanism that allows privileged transfer of Ca^{2+} from the ER to mitochondria. Indeed, it has been shown

that the ER and mitochondria make close contacts (10–30 nm in distance), and that such contact sites are crucial for efficient Ca^{2+} transfer (Rizzuto et al., 1998; de Brito and Scorrano, 2010; Hirabayashi et al., 2017). This finding suggests that IP_3R2-independent Ca^{2+} release is capable of increasing $[Ca^{2+}]_{Cyt}$ within close proximity to the ER membrane, generating Ca^{2+} nanodomains around the ER (Rizzuto and Pozzan, 2006). Thus, in addition to extracellular and mitochondrial sources of Ca^{2+} for localized Ca^{2+} signaling (Srinivasan et al., 2015; Agarwal et al., 2017), IP_3R2-independent Ca^{2+} release may contribute to Ca^{2+} signaling in IP_3R2-KO astrocytes.

We also noted the spatial distribution of IP_3R2-independent Ca^{2+} release, which was observed throughout the cell including the soma and processes in NE-stimulated IP_3R2-KO astrocytes (Fig. 2). This compares with the subcellular-confined Ca^{2+} signals within the processes due to Ca^{2+} influx from the extracellular space or Ca^{2+} release from mitochondria in IP_3R2-KO astrocytes in the absence of agonist stimulation (Kanemaru et al., 2014; Srinivasan et al., 2015; Agarwal et al., 2017). Therefore, IP_3R2-independent Ca^{2+} release may have distinct roles, especially in the somatic region of IP_3R2-KO astrocytes.

Reinterpretation of astrocytic functions in IP_3R2-KO mice

It has been assumed that Ca^{2+} release from the ER is absent in IP_3R2-KO astrocytes. Thus, the absence of functional deficits in IP_3R2-KO mice (Petravicz et al., 2008, 2014, Agulhon et al., 2010, 2013; Nizar et al., 2013; Takata et al., 2013; Bonder and McCarthy, 2014) has been considered to indicate the absence of functional roles of intracellular Ca^{2+} release in astrocytes. The presence of IP_3R2-independent Ca^{2+} release may necessitate reinterpretation of such results.

Ca^{2+} release from the ER may be inhibited by expressing the IP_3 hydrolyzing enzyme, IP_3 5-phosphatase (5ppase) (Kanemaru et al., 2007; Mashimo et al., 2010; Foley et al., 2017).

Indeed, exogenous expression of 5ppase effectively suppresses IP_3 production following IP_3R-dependent Ca^{2+} release in astrocytes (Kanemaru et al., 2007; Mashimo et al., 2010). Because 5ppase is expected to suppress IP_3R-induced Ca^{2+} release regardless of IP_3R subtypes, the phenotypic difference between 5ppase-expressing mice and IP_3R2-KO mice may clarify the role of IP_3R2-independent Ca^{2+} release. In fact, a recent study has indicated that astrocytic expression of 5ppase disrupts sleep (Foley et al., 2017), whereas sleep disruption was not observed in IP_3R2-KO mice (Cao et al., 2013). Although there remains the possibility of developmental adaptation or other compensatory mechanisms in these mice, the results suggest that residual Ca^{2+} signaling, including IP_3R2-independent Ca^{2+} release in IP_3R2-KO mice, accounts for the absence of functional deficits in IP_3R2-KO mice.

In conclusion, the presence of IP_3R2-independent Ca^{2+} release as well as Ca^{2+} signaling generated by sources other than the ER limit the use of IP_3R2-KO mice to assess the role of Ca^{2+} signaling in astrocytic functions when functional deficits are not observed in the mutant mice. This notion may help to resolve the long-lasting controversy arising from the assumption that Ca^{2+} signaling is abolished in IP_3R2-KO astrocytes. Furthermore, the present results facilitate the study of the functional roles of Ca^{2+} signaling in close proximity to the ER in astrocytes.

Acknowledgements

We thank Y. Kawashima for technical assistance and Dr. B. Khakh (University of California at San Francisco) for providing the pZac2.1-gfaABC1D-Lck-GCaMP3 plasmid. This work was supported by the Japan Society for the Promotion of Science (JSPS) KAKENHI [Grant Numbers JP16K08543 (Y.O.), JP15H05648 (K.K.), and JP21229004 and JP25221304 (M.I.)] and grants from the Tokyo Society of Medical Sciences (Y.O.).

References

Agarwal A, Wu P-H, Hughes EG, Fukaya M, Tischfield MA, Langseth AJ, Wirtz D, Bergles DE (2017) Transient opening of the mitochondrial permeability transition pore induces microdomain calcium transients in astrocyte processes. Neuron 93:587–605.

Agulhon C, Boyt KM, Xie AX, Friocourt F, Roth BL, McCarthy KD (2013) Modulation of the autonomic nervous system and behaviour by acute glial cell G_q protein-coupled receptor activation in vivo. J Physiol 591:5599–5609.

Agulhon C, Fiacco TA, McCarthy KD (2010) Hippocampal short- and long-term plasticity are not modulated by astrocyte Ca^{2+} signaling. Science (80-) 327:1250–1254.

Barres BA (2008) The mystery and magic of glia: a perspective on their roles in health and disease. Neuron 60:430–440.

Bazargani N, Attwell D (2016) Astrocyte calcium signaling: the third wave. Nat Neurosci 19:182–189.

Bonder DE, McCarthy KD (2014) Astrocytic G_q-GPCR-linked IP_3R-dependent Ca^{2+} signaling does not mediate neurovascular coupling in mouse visual cortex *in vivo*. J Neurosci 34:13139–13150.

Cahoy JD, Emery B, Kaushal A, Foo LC, Zamanian JL, Christopherson KS, Xing Y, Lubischer JL, Krieg PA, Krupenko SA, Thompson WJ, Barres BA (2008) A transcriptome database for astrocytes, neurons, and oligodendrocytes: a new resource for understanding brain development and function. J Neurosci 28:264–278.

Cao X, Li L-P, Wang Q, Wu Q, Hu H-H, Zhang M, Fang Y-Y, Zhang J, Li S-J, Xiong W-C, Yan H-C, Gao Y-B, Liu J-H, Li X-W, Sun L-R, Zeng Y-N, Zhu X-H, Gao T-M (2013) Astrocyte-derived ATP modulates depressive-like behaviors. Nat Med 19:773–777.

Chai H, Diaz-Castro B, Shigetomi E, Monte E, Octeau JC, Yu X, Cohn W, Rajendran PS, Vondriska TM, Whitelegge JP, Coppola G, Khakh BS (2017) Neural circuit-specialized astrocytes: transcriptomic, proteomic, morphological, and functional evidence. Neuron 95:531–549.

Chen N, Sugihara H, Sharma J, Perea G, Petravicz J, Le C, Sur M (2012) Nucleus basalis-enabled stimulus-specific plasticity in the visual cortex is mediated by astrocytes. Proc Natl Acad Sci 109:E2832–E2841.

Chen T-W, Wardill TJ, Sun Y, Pulver SR, Renninger SL, Baohan A, Schreiter ER, Kerr RA, Orger MB, Jayaraman V, Looger LL, Svoboda K, Kim DS (2013) Ultrasensitive fluorescent proteins for imaging neuronal activity. Nature 499:295–300.

de Brito OM, Scorrano L (2010) An intimate liaison: spatial organization of the endoplasmic reticulum-mitochondria relationship. EMBO J 29:2715–2723.

Ding F, O'Donnell J, Thrane AS, Zeppenfeld D, Kang H, Xie L, Wang F, Nedergaard M (2013) α1-Adrenergic receptors mediate coordinated Ca^{2+} signaling of cortical astrocytes in awake, behaving mice. Cell Calcium 54:387–394.

Dong Q, He J, Chai Z (2013) Astrocytic Ca^{2+} waves mediate activation of extrasynaptic NMDA receptors in hippocampal neurons to aggravate brain damage during ischemia. Neurobiol Dis 58:68–75.

Edwards FA, Konnerth A, Sakmann B, Takahashi T (1989) A thin slice preparation for patch clamp recordings from neurones of the mammalian central nervous system. Pflugers Arch 414:600–612.

Fiacco TA, McCarthy KD (2018) Multiple lines of evidence indicate that gliotransmission does not occur under physiological conditions. J Neurosci 38:3–13.

Foley J, Blutstein T, Lee S, Erneux C, Halassa MM, Haydon P (2017) Astrocytic IP_3/Ca^{2+} signaling modulates theta rhythm and REM sleep. Front Neural Circuits 11:3.

Hamilton NB, Attwell D (2010) Do astrocytes really exocytose neurotransmitters? Nat Rev Neurosci 11:227–238.

Hirabayashi Y, Kwon S-K, Paek H, Pernice WM, Paul MA, Lee J, Erfani P, Raczkowski A, Petrey DS, Pon LA, Polleux F (2017) ER-mitochondria tethering by PDZD8 regulates Ca^{2+} dynamics in mammalian neurons. Science 358:623–630.

Holtzclaw LA, Pandhit S, Bare DJ, Mignery GA, Russell JT (2002) Astrocytes in adult rat brain express type 2 inositol 1,4,5-trisphosphate receptors. Glia 39:69–84.

Kanemaru K, Kubota J, Sekiya H, Hirose K, Okubo Y, Iino M (2013) Calcium-dependent N-cadherin up-regulation mediates reactive astrogliosis and neuroprotection after brain injury. Proc Natl Acad Sci 110:11612–11617.

Kanemaru K, Okubo Y, Hirose K, Iino M (2007) Regulation of neurite growth by spontaneous Ca^{2+} oscillations in astrocytes. J Neurosci 27:8957–8966.

Kanemaru K, Sekiya H, Xu M, Satoh K, Kitajima N, Yoshida K, Okubo Y, Sasaki T, Moritoh S, Hasuwa H, Mimura M, Horikawa K, Matsui K, Nagai T, Iino M, Tanaka KF (2014) *In vivo* visualization of subtle, transient, and local activity of astrocytes using an ultrasensitive Ca^{2+} indicator. Cell Rep 8:311–318.

Kim SK, Hayashi H, Ishikawa T, Shibata K, Shigetomi E, Shinozaki Y, Inada H, Roh SE, Kim SJ, Lee G, Bae H, Moorhouse AJ, Mikoshiba K, Fukazawa Y, Koizumi S, Nabekura J (2016) Cortical astrocytes rewire somatosensory cortical circuits for peripheral neuropathic pain. J Clin Invest 126:1983–1997.

Li H, Xie Y, Zhang N, Yu Y, Zhang Q, Ding S (2015) Disruption of IP_3R2-mediated Ca^{2+} signaling pathway in astrocytes ameliorates neuronal death and brain damage while

reducing behavioral deficits after focal ischemic stroke. Cell Calcium 58:565–576.

Li X, Zima A V., Sheikh F, Blatter LA, Chen J (2005) Endothelin-1–induced arrhythmogenic Ca^{2+} signaling is abolished in atrial myocytes of inositol-1,4,5-trisphosphate (IP_3)–receptor type 2–deficient mice. Circ Res 96:1274–1281.

Mashimo M, Okubo Y, Yamazawa T, Yamasaki M, Watanabe M, Murayama T, Iino M (2010) Inositol 1,4,5-trisphosphate signaling maintains the activity of glutamate uptake in Bergmann glia. Eur J Neurosci 32:1668–1677.

Matyash M, Matyash V, Nolte C, Sorrentino V, Kettenmann H (2002) Requirement of functional ryanodine receptor type 3 for astrocyte migration. FASEB J 16:84–86.

Mogami H, Gardner J, Gerasimenko O, Camello P, Petersen O, Tepikin A (1999) Calcium binding capacity of the cytosol and endoplasmic reticulum of mouse pancreatic acinar cells. J Physiol 518:463–467.

Monai H, Ohkura M, Tanaka M, Oe Y, Konno A, Hirai H, Mikoshiba K, Itohara S, Nakai J, Iwai Y, Hirase H (2016) Calcium imaging reveals glial involvement in transcranial direct current stimulation-induced plasticity in mouse brain. Nat Commun 7:11100.

Navarrete M, Perea G, de Sevilla DF, Gómez-Gonzalo M, Núñez A, Martín ED, Araque A (2012) Astrocytes mediate *in vivo* cholinergic-induced synaptic plasticity. PLoS Biol 10:e1001259.

Neher E (1995) The use of fura-2 for estimating Ca buffers and Ca fluxes. Neuropharmacology 34:1423–1442.

Nizar K et al. (2013) *In vivo* stimulus-induced vasodilation occurs without IP_3 receptor activation and may precede astrocytic calcium increase. J Neurosci 33:8411–8422.

Okubo Y, Suzuki J, Kanemaru K, Nakamura N, Shibata T, Iino M (2015) Visualization of Ca^{2+} filling mechanisms upon synaptic inputs in the endoplasmic reticulum of cerebellar Purkinje cells. J Neurosci 35:15837–15846.

Padmashri R, Suresh A, Boska MD, Dunaevsky A (2015) Motor-skill learning is dependent on astrocytic activity. Neural Plast 2015:938023.

Patrushev I, Gavrilov N, Turlapov V, Semyanov A (2013) Subcellular location of astrocytic calcium stores favors extrasynaptic neuron–astrocyte communication. Cell Calcium 54:343–349.

Paukert M, Agarwal A, Cha J, Doze VA, Kang JU, Bergles DE (2014) Norepinephrine controls astroglial responsiveness to local circuit activity. Neuron 82:1263–1270.

Paumgartner D, Losa G, Weibel ER (1981) Resolution effect on the stereological estimation of surface and volume and its interpretation in terms of fractal dimensions. J Microsc 121:51–63.

Perez-Alvarez A, Navarrete M, Covelo A, Martin ED, Araque A (2014) Structural and functional plasticity of astrocyte processes and dendritic spine interactions. J Neurosci 34:12738–12744.

Petravicz J, Boyt KM, McCarthy KD (2014) Astrocyte IP_3R2-dependent Ca^{2+} signaling is not a major modulator of neuronal pathways governing behavior. Front Behav Neurosci 8:384.

Petravicz J, Fiacco TA, McCarthy KD (2008) Loss of IP_3 receptor-dependent Ca^{2+} increases in hippocampal astrocytes does not affect baseline CA1 pyramidal neuron synaptic activity. J Neurosci 28:4967–4973.

Rakers C, Petzold GC (2016) Astrocytic calcium release mediates peri-infarct depolarizations in a rodent stroke model. J Clin Invest 127:511–516.

Rizzuto R, Pinton P, Carrington W, Fay FS, Fogarty KE, Lifshitz LM, Tuft RA, Pozzan T (1998) Close contacts with the endoplasmic reticulum as determinants of mitochondrial Ca^{2+} responses. Science 280:1763–1766.

Rizzuto R, Pozzan T (2006) Microdomains of intracellular Ca^{2+}: molecular determinants and functional consequences. Physiol Rev 86:369–408.

Rungta RL, Bernier L-P, Dissing-Olesen L, Groten CJ, LeDue JM, Ko R, Drissler S, MacVicar BA (2016) Ca^{2+} transients in astrocyte fine processes occur via Ca^{2+} influx in the adult mouse hippocampus. Glia 64:2093–2103.

Saito K, Shigetomi E, Yasuda R, Sato R, Nakano M, Tashiro K, Tanaka KF, Ikenaka K, Mikoshiba K, Mizuta I, Yoshida T, Nakagawa M, Mizuno T, Koizumi S (2018) Aberrant astrocyte Ca2+ signals “AxCa signals” exacerbate pathological alterations in an Alexander disease model. Glia 66:1053–1067.

Savtchouk I, Volterra A (2018) Gliotransmission: beyond black-and-white. J Neurosci 38:14–25.

Sharp AH, Nucifora FC, Blondel O, Sheppard CA, Zhang C, Snyder SH, Russell JT, Ryugo DK, Ross CA (1999) Differential cellular expression of isoforms of inositol 1,4,5-triphosphate receptors in neurons and glia in brain. J Comp Neurol 406:207–220.

Sherwood MW, Arizono M, Hisatsune C, Bannai H, Ebisui E, Sherwood JL, Panatier A, Oliet SHR, Mikoshiba K (2017) Astrocytic IP_3Rs: contribution to Ca^{2+} signalling and hippocampal LTP. Glia 65:502–513.

Shigetomi E, Bushong EA, Haustein MD, Tong X, Jackson-Weaver O, Kracun S, Xu J, Sofroniew M V., Ellisman MH, Khakh BS (2013) Imaging calcium microdomains within entire astrocyte territories and endfeet with GCaMPs expressed using adeno-associated viruses. J Gen Physiol 141:633–647.

Shigetomi E, Tong X, Kwan KY, Corey DP, Khakh BS (2012) TRPA1 channels regulate astrocyte resting calcium and inhibitory synapse efficacy through GAT-3. Nat Neurosci 15:70–80.

Srinivasan R, Huang BS, Venugopal S, Johnston AD, Chai H, Zeng H, Golshani P, Khakh BS (2015) Ca^{2+} signaling in astrocytes from *Ip3r2*$^{-/-}$ mice in brain slices and during startle responses *in vivo*. Nat Neurosci 18:708–717.

Suzuki J, Kanemaru K, Iino M (2016) Genetically encoded fluorescent indicators for organellar calcium imaging. Biophys J 111:1119–1131.

Suzuki J, Kanemaru K, Ishii K, Ohkura M, Okubo Y, Iino M (2014) Imaging intraorganellar Ca^{2+} at subcellular resolution using CEPIA. Nat Commun 5:4153.

Takata N, Mishima T, Hisatsune C, Nagai T, Ebisui E, Mikoshiba K, Hirase H (2011) Astrocyte calcium signaling transforms cholinergic modulation to cortical plasticity *in vivo*. J Neurosci 31:18155–18165.

Takata N, Nagai T, Ozawa K, Oe Y, Mikoshiba K, Hirase H (2013) Cerebral blood flow modulation by basal forebrain or whisker stimulation can occur independently of large cytosolic Ca^{2+} signaling in astrocytes. PLoS One 8:e66525.

Tamamushi S, Nakamura T, Inoue T, Ebisui E, Sugiura K, Bannai H, Mikoshiba K (2012) Type 2 inositol 1,4,5-trisphosphate receptor is predominantly involved in agonist-induced Ca^{2+} signaling in Bergmann glia. Neurosci Res 74:32–41.

Verkhratsky A, Orkand RK, Kettenmann H (1998) Glial calcium: homeostasis and signaling function. Physiol Rev 78:99–141.

Volterra A, Meldolesi J (2005) Astrocytes, from brain glue to communication elements: the revolution continues. Nat Rev Neurosci 6:626–640.

Wang F, Smith NA, Xu Q, Fujita T, Baba A, Matsuda T, Takano T, Bekar L, Nedergaard M (2012a) Astrocytes modulate neural network activity by Ca^{2+}-dependent uptake of extracellular K^{+}. Sci Signal 5:ra26.

Wang F, Xu Q, Wang W, Takano T, Nedergaard M (2012b) Bergmann glia modulate cerebellar Purkinje cell bistability via Ca^{2+}-dependent K^{+} uptake. Proc Natl Acad Sci U S A 109:7911–7916.

Yamamoto-Hino M, Miyawaki A, Kawano H, Sugiyama T, Furuichi T, Hasegawa M, Mikoshiba K (1995) Immunohistochemical study of inositol 1,4,5-trisphosphate receptor type 3 in rat central nervous system. Neuroreport 6:273–276.

Yang J, Yang H, Liu Y, Li X, Qin L, Lou H, Duan S, Wang H (2016) Astrocytes contribute to synapse elimination *via* type 2 inositol 1,4,5-trisphosphate receptor-dependent release of ATP. Elife 5:e15043.

Zhang Y, Chen K, Sloan SA, Bennett ML, Scholze AR, O'Keeffe S, Phatnani HP, Guarnieri P, Caneda C, Ruderisch N, Deng S, Liddelow SA, Zhang C, Daneman R, Maniatis T, Barres BA, Wu JQ (2014) An RNA-sequencing transcriptome and splicing database of glia, neurons, and vascular cells of the cerebral cortex. J Neurosci 34:11929–11947.

Figure legends

Figure 1. Ca^{2+} imaging within the ER of cortical astrocytes using G-CEPIA1*er*.

(A) Immunohistochemical analysis of G-CEPIA1*er*-expressing astrocytes in the cortex. G-CEPIA1*er* shows colocalization with the astrocyte marker GFAP. Scale bar, 20 μm.

(B) SERCA inhibitor-induced Ca^{2+} depletion confirmed that G-CEPIA1*er* reflected $[Ca^{2+}]_{ER}$. Representative $\Delta F/F_0$ traces and summarized graphs indicated the same amplitude of G-CEPIA1*er* fluorescence decrease upon application of CPA (50 μM, gray bar) to WT (black trace) and IP_3R2-KO (magenta trace) astrocytes. A whole astrocyte was selected as the region of interest to measure $\Delta F/F_0$. n = 23 cells for WT and 21 cells for IP_3R2-KO (mean ± s.e.m.).

Figure 2. IP_3R2-independent Ca^{2+} release in cortical astrocytes.

(A) Representative G-CEPIA1*er* responses in the soma and processes upon application of NE (10 μM, cyan bars) to WT (black traces) and IP_3R2-KO (magenta traces) astrocytes in cortical slices. Regions enclosed by yellow circles in left images indicate the somatic and process regions of interest for $\Delta F/F_0$ traces. Scale bar, 10 μm.

(B) G-CEPIA1*er* responses in the soma and processes upon application of NE (10 μM, cyan bars) to WT (black) and IP_3R2-KO (magenta) astrocytes. Individual $\Delta F/F_0$ traces (pale color) and average traces (deep color) are indicated. n = 11 cells for WT and 12 cells for IP_3R2-KO.

(C) ER-YFP showed no response to NE (10 μM, cyan bars) in both WT (black) and IP_3R2-KO (magenta) astrocytes, indicating no Ca^{2+}-independent changes of fluorescent proteins. A whole astrocyte was selected as the region of interest to measure $\Delta F/F_0$. Individual $\Delta F/F_0$ traces (pale color) and average traces (deep color) are indicated. n = 12 cells for WT and 10 cells for IP_3R2-KO.

(D) Summarized graph of the response amplitudes of $\Delta F/F_0$ traces shown in (B) and (C) (mean ± s.e.m.), indicating attenuated but significant G-CEPIA1*er* responses in IP_3R2-KO

astrocytes as well as the same responses between the soma and processes.

Figure 3. Spontaneous ER Ca^{2+} release in cortical astrocytes.

(A) Representative spontaneous G-CEPIA1*er* responses that emerged synchronously throughout a WT astrocyte (global response). The yellow circle enclosing an astrocyte in the left image indicates the region of interest for the bottom $\Delta F/F_0$ trace. Pseudocolor images indicate the average of $\Delta F/F_0$ in five consecutive frames at the time points indicated by gray bars in the bottom $\Delta F/F_0$ trace. Scale bar, 20 μm.

(B) Representative spontaneous G-CEPIA1*er* responses that emerged in confined regions of processes in a WT astrocyte (process-localized response). Yellow circles and numbers in the left image correspond to the bottom $\Delta F/F_0$ traces. Pseudocolor $\Delta F/F_0$ images indicate the spatiotemporal distribution of responses. Scale bar, 20 μm.

(C) Representative non-spontaneous G-CEPIA1*er* responses in an IP_3R2-KO astrocyte. The yellow circle enclosing an astrocyte in the left image indicates the region of interest for the bottom $\Delta F/F_0$ trace. Pseudocolor $\Delta F/F_0$ images indicate no response. Scale bar, 20 μm.

(D) Summary of frequencies (left) and amplitudes (right) of global and process-localized responses in WT astrocytes. n = 25 global responses and 27 process-localized responses in 15 cells (mean ± s.e.m.).

Figure 4. Cytosolic Ca^{2+} transients induced by IP_3R2-independent Ca^{2+} release.

(A) GCaMP6f-expressing astrocyte. Scale bar, 10 μm.

(B) GCaMP6f responses upon application of NE (10 μM, cyan bars) to WT (black) and IP_3R2-KO (magenta) astrocytes in the control condition [CPA (−)] or after treatment with CPA [CPA (+)]. A whole astrocyte was selected as the region of interest to measure $\Delta F/F_0$. Individual $\Delta F/F_0$ traces (pale color) and average traces (deep color) are indicated. n = 13 cells

for WT [CPA (−)], 10 cells for WT [CPA (+)], 16 cells for IP_3R2-KO [CPA (−)], and 10 cells for IP_3R2-KO [CPA (+)].

(C) Summarized graph of the response amplitudes of $\Delta F/F_0$ traces shown in (B) (mean ± s.e.m.), indicating weak GCaMP6f responses in IP_3R2-KO astrocytes. Abolishment of responses by CPA indicated the contribution of ER Ca^{2+} release to GCaMP6f responses.

Figure 5. Mitochondrial Ca^{2+} transients induced by IP_3R2-independent Ca^{2+} release.

(A) CEPIA2*mt*-expressing astrocyte. Scale bar, 10 μm.

(B) CEPIA2*mt* responses upon application of NE (10 μM, cyan bars) to WT (black) and IP_3R2-KO (magenta) astrocytes in the control condition [CPA (−)] or after treatment with CPA [CPA (+)]. A whole astrocyte was selected as the region of interest to measure $\Delta F/F_0$. Individual $\Delta F/F_0$ traces (pale color) and average traces (deep color) are indicated. n = 18 cells for WT [CPA (−)], 10 cells for WT [CPA (+)], 16 cells for IP_3R2-KO [CPA (−)], and 12 cells for IP_3R2-KO [CPA (+)].

(C) Summarized graph of the response amplitudes of $\Delta F/F_0$ traces shown in (B) (mean ± s.e.m.), indicating attenuated but significant CEPIA2*mt* responses in IP_3R2-KO astrocytes. Abolishment of responses by CPA indicated the contribution of ER Ca^{2+} release to CEPIA2*mt* responses.

Figure 6. IP_3R2-independent Ca^{2+} release in hippocampal astrocytes.

(A) Representative spontaneous global G-CEPIA1*er* responses in a hippocampal WT astrocyte. The yellow circle enclosing an astrocyte in the left image indicates the region of interest for the $\Delta F/F_0$ trace. Scale bar, 10 μm.

(B) Representative spontaneous process-localized G-CEPIA1*er* responses in a hippocampal WT astrocyte. Yellow circles and numbers in the left image correspond to the $\Delta F/F_0$ traces.

Scale bar, 10 μm.

(C) Representative non-spontaneous G-CEPIA1*er* responses in a hippocampal IP_3R2-KO astrocyte. The yellow circle enclosing an astrocyte in the left image indicates the region of interest for the $\Delta F/F_0$ trace. Scale bar, 10 μm.

(D) Summary of frequencies and amplitudes (E) of global and process-localized responses in hippocampal WT astrocytes. n = 29 global responses and 27 process-localized responses in 16 cells (mean ± s.e.m.).

(E) G-CEPIA1*er* responses upon application of NE (10 μM, cyan bars) to WT (black) and IP_3R2-KO (magenta) astrocytes. A whole astrocyte was selected as the region of interest to measure $\Delta F/F_0$. Individual $\Delta F/F_0$ traces (pale color) and average traces (deep color) are indicated. n = 16 cells for WT and 18 cells for IP_3R2-KO. Left graph is a summary of the response amplitudes of $\Delta F/F_0$ traces (mean ± s.e.m.), indicating attenuated but significant G-CEPIA1*er* responses in IP_3R2-KO astrocytes.

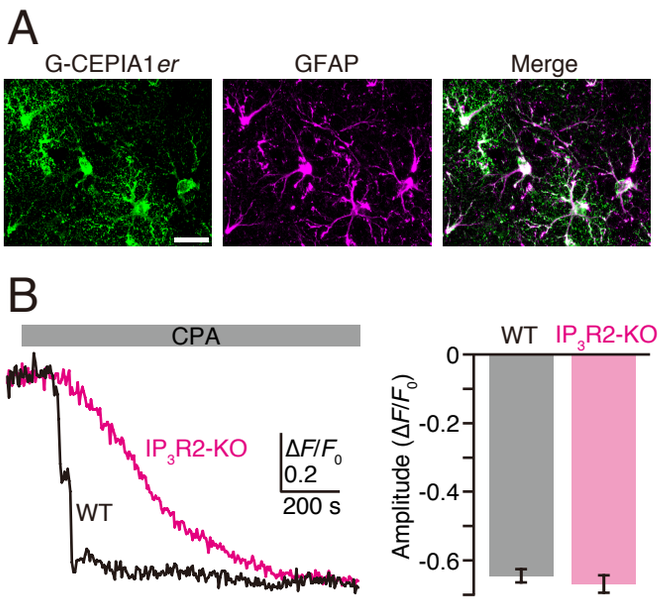
A
G-CEPIA1er
GFAP
Merge
B
CPA
IP3R2-KO
WT
ΔF/F0
0.2
200 s
WT
IP3R2-KO
Amplitude (ΔF/F0)
0
-0.2
-0.4
-0.6

Fig. 1

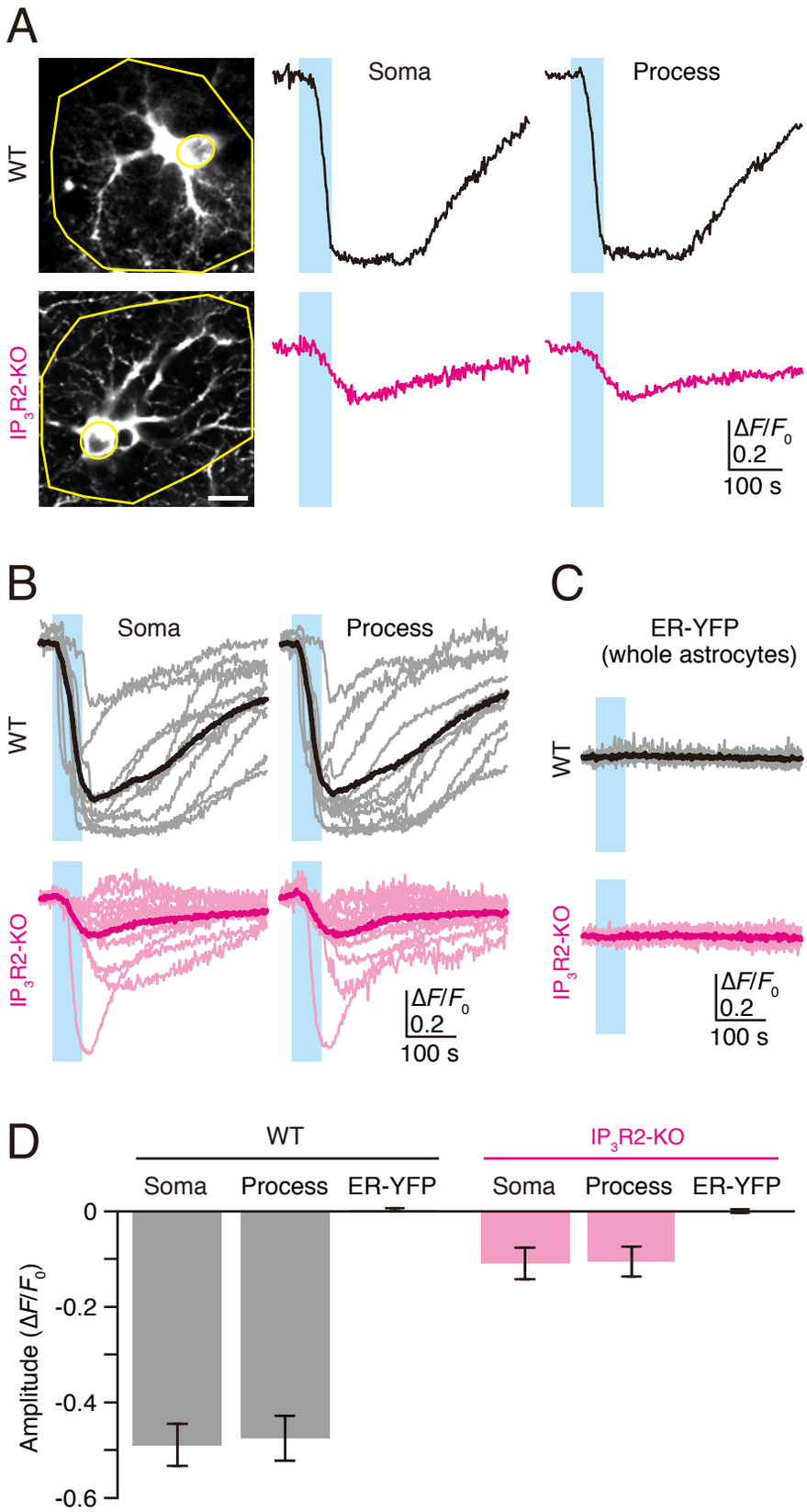
A
WT
IP3R2-KO
Soma
Process
ΔF/F0
0.2
100 s
B
Soma
Process
WT
IP3R2-KO
ΔF/F0
0.2
100 s
C
ER-YFP
(whole astrocytes)
WT
IP3R2-KO
ΔF/F0
0.2
100 s
D
WT
IP3R2-KO
Soma
Process
ER-YFP
Soma
Process
ER-YFP
Amplitude (ΔF/F0)
0
-0.2
-0.4
-0.6

Fig. 2

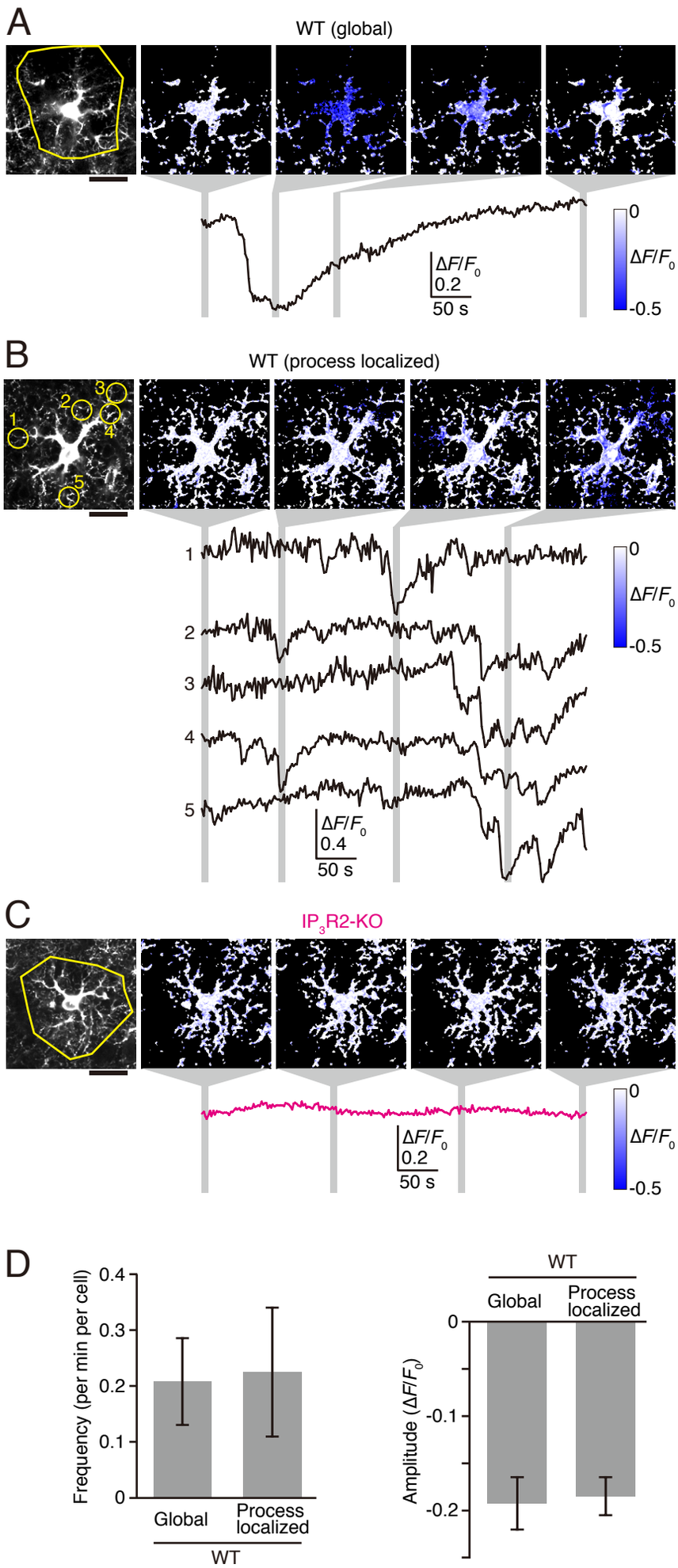
A
WT (global)
ΔF/F0
0.2
50 s
0
ΔF/F0
-0.5
B
WT (process localized)
1
2
3
4
5
ΔF/F0
0.4
50 s
C
IP3R2-KO
ΔF/F0
0.2
50 s
D
Frequency (per min per cell)
0.4
0.3
0.2
0.1
0
Global
Process localized
WT
Amplitude (ΔF/F0)
0
-0.1
-0.2

Fig. 3

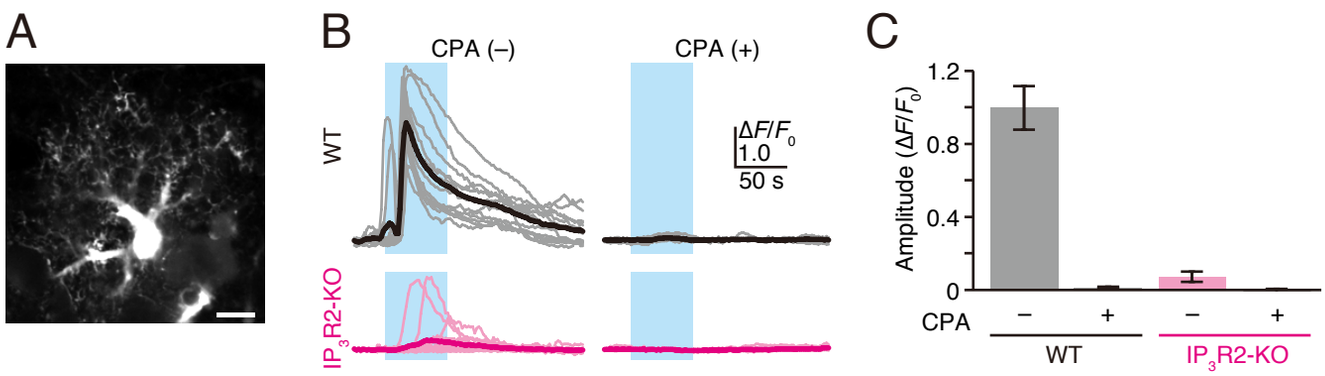
A
B
CPA (–)
CPA (+)
WT
IP3R2-KO
ΔF/F0
1.0
50 s
C
Amplitude (ΔF/F0)
1.2
0.8
0.4
0
CPA
–
+
–
+
WT
IP3R2-KO

Fig. 4

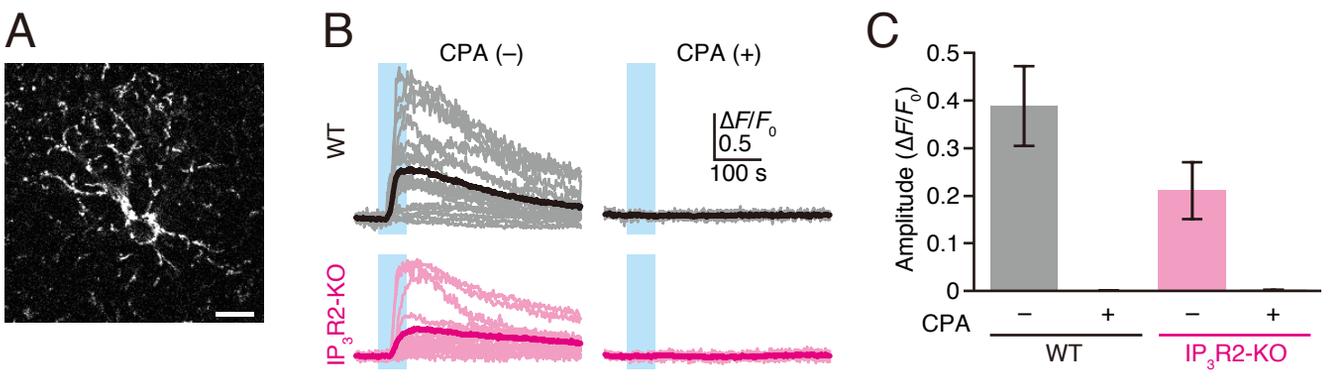
A
B
CPA (–)
CPA (+)
WT
IP3R2-KO
ΔF/F0
0.5
100 s
C
Amplitude (ΔF/F0)
0.5
0.4
0.3
0.2
0.1
0
CPA
–
+
–
+
WT
IP3R2-KO

Fig. 5

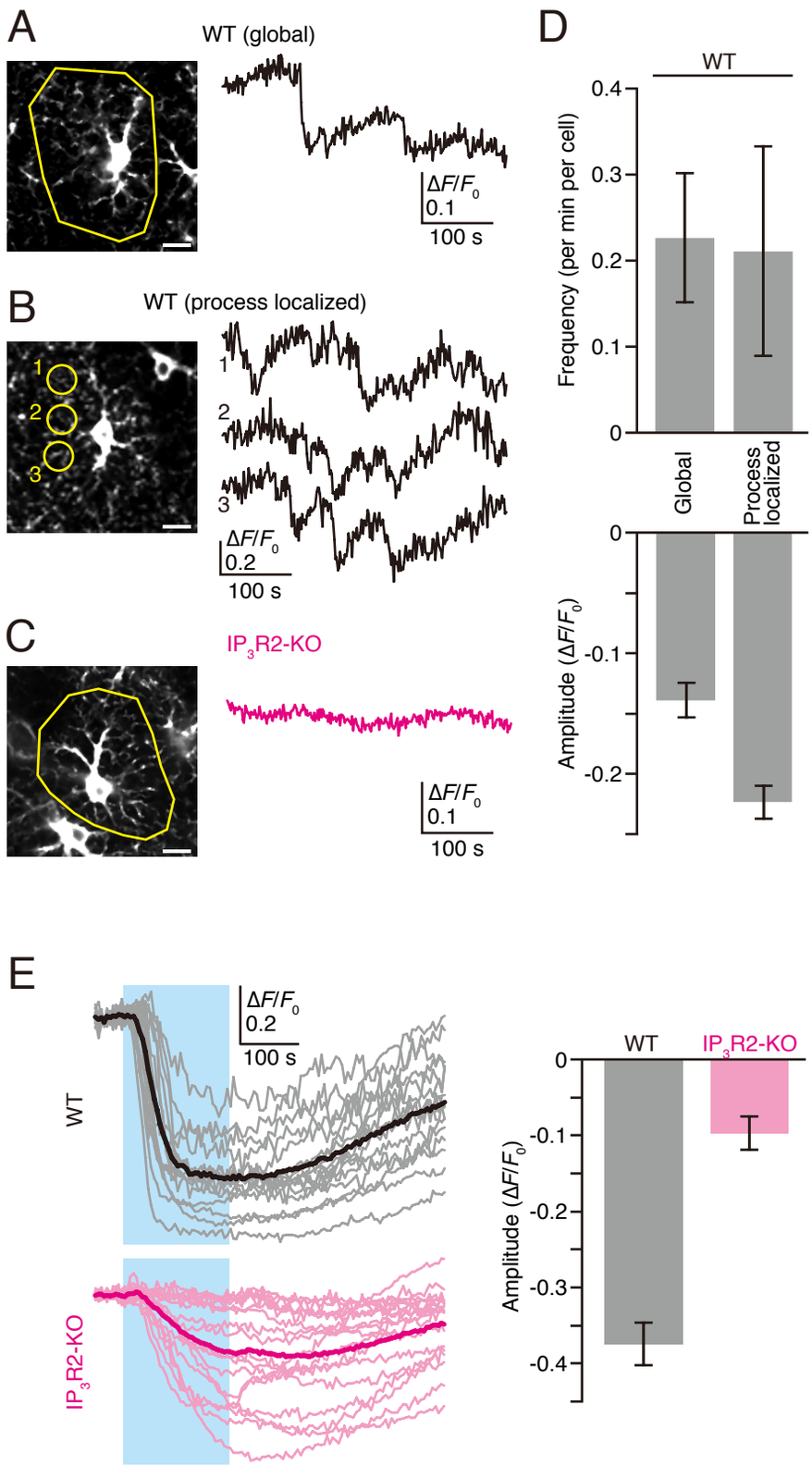
A
WT (global)
ΔF/F0
0.1
100 s
B
WT (process localized)
1
2
3
ΔF/F0
0.2
100 s
C
IP3R2-KO
ΔF/F0
0.1
100 s
D
WT
Frequency (per min per cell)
0.4
0.3
0.2
0.1
0
Global
Process localized
Amplitude (ΔF/F0)
0
-0.1
-0.2
E
ΔF/F0
0.2
100 s
WT
IP3R2-KO
WT
IP3R2-KO
Amplitude (ΔF/F0)
0
-0.1
-0.2
-0.3
-0.4

Fig. 6